THE JOURNAL OF BIOLOGICAL CHEMISTRY
Vol. 280, No. 34, Issue of August 26, pp. 30574–30580, 2005

Printed in U.S.A.

Siderophore Transport through *Escherichia coli* Outer Membrane Receptor FhuA with Disulfide-tethered Cork and Barrel Domains*

Received for publication, June 20, 2005
Published, JBC Papers in Press, June 30, 2005, DOI 10.1074/jbc.M506708200

H. Anne Eisenhauer, Sofia Shames, Peter D. Pawelek, and James W. Coulton‡

From the Department of Microbiology and Immunology, McGill University, Montreal, Quebec H3A 2B4, Canada

The hydroxamate siderophore receptor FhuA is a TonB-dependent outer membrane protein of *Escherichia coli* composed of a C-terminal 22-stranded β-barrel occluded by an N-terminal globular cork domain. During siderophore transport into the periplasm, the FhuA cork domain has been proposed to undergo conformational changes that allow transport through the barrel lumen; alternatively, the cork may be completely displaced from the barrel. To probe such changes, site-directed cysteine mutants in the cork domain (L109C and Q112C) and in the barrel domain (S356C and M383C) were created within the putative siderophore transport pathway. Molecular modeling predicted that the double cysteine mutants L109C/S356C and Q112C/M383C would form disulfide bonds, thereby tethering the cork and barrel domains. The double cysteine FhuA mutants were denatured under nonreducing conditions and fluorescently labeled with thiol-specific Oregon Green maleimide. Subsequent SDS-PAGE analysis revealed two distinct species: FhuA containing a disulfide bond and FhuA with free sulfhydryl groups. To address the role of the putative siderophore transport pathway and to evaluate possible rearrangements of the cork domain during ferricrocin transport, disulfide bond formation was enhanced by an oxidative catalyst. Cells containing double cysteine FhuA mutants that were subjected to oxidation during ferricrocin transport exhibited disulfide bond formation to near completion. After disulfide tethering of the cork to the barrel, ferricrocin transport was equivalent to transport by untreated cells. These results demonstrate that blocking the putative siderophore transport pathway does not abrogate ferricrocin uptake. We propose that, during siderophore transport through FhuA, the cork domain remains within the barrel rather than being displaced.

Iron is required by most living cells because of its diverse roles in numerous metabolic processes, including glycolysis, energy generation by electron transport, and DNA synthesis (1). Under physiological conditions, however, iron forms highly insoluble ferric hydroxide complexes, thereby severely limiting the bioavailability of iron. The outer membrane receptor FhuA of *Escherichia coli* transports Fe^{3+} chelated to hydroxamate siderophores such as ferrichrome and its structural analog ferricrocin. FhuA also serves as a primary receptor for the antibiotics albomycin and rifamycin CGP 4832; the antibiotic peptide microcin J25; the bacterial toxin colicin M; and the bacteriophages T5, T1, UC-1, and Φ80. Structural determination of FhuA identified a monomeric C-terminal 22-stranded β-barrel domain (residues 161–714) and an N-terminal globular cork domain (residues 1–160) that resides within the barrel lumen (2, 3). The position of the cork domain within the barrel occludes the barrel lumen and prevents diffusion of ligand into the periplasm. The mechanism by which this occlusion is modulated to facilitate siderophore transport remains unclear.

Ferric siderophore transport requires a pathway with a minimal diameter of ~15 Å, which is not apparent in either apo-FhuA (Protein Data Bank code 2FCP) or the ferrichrome-bound crystal structure (Protein Data Bank code 1FCP) (1, 4). Comparison of these two FhuA structures revealed distinct conformations; most differences are localized to the cork domain, thereby providing direct evidence for conformational changes that occur within FhuA upon ligand binding. In the ferrichrome-bound state, apices in the cork domain are translated 1.7 Å toward the ferrichrome-binding site, forming multiple hydrogen bonds with the ligand (2, 3). The most conspicuous structural change takes place in an N-terminal region referred to as the switch helix. Upon ferrichrome binding to FhuA, the switch helix is entirely unwound, resulting in a 17.3-Å translocation of the N terminus (2). Despite these changes in the ferrichrome-bound state, a transport pathway sufficient to accommodate a siderophore remains undetected. Therefore, after siderophore binding, the additional structural alterations that FhuA must undergo to allow passage of ligand though the barrel lumen are as yet undisclosed by x-ray crystallographic structures.

Proposed models of siderophore transport through FhuA involve subtle rearrangement(s) of the cork domain; alternatively, complete or partial removal of the cork domain from the barrel has been postulated (1, 4–6). Transport into the periplasm requires reduced stability of ferrichrome for its initial binding site, eventually facilitating dissociation from the outer membrane receptor. In ferrichrome-bound FhuA, the N-terminal region of the receptor interacts with the energy-transducing complex TonB-ExbB-ExbD anchored in the cytoplasmic membrane. Selected residues of the Ton box, a sequence of amino acids highly conserved among TonB-dependent outer membrane receptors, make direct interactions with TonB as demonstrated by disulfide cross-linking (7). These interactions are not only required for transport, but are likely coupled to conformational changes in the cork and barrel during transport (8). Such conformational changes have been proposed to destabilize ferrichrome contacts with extracellular loops of the bar-

* This work was supported by operating grants from the Natural Sciences and Engineering Research Council of Canada and the Canadian Institutes of Health Research (to J. W. C.). The Canada Foundation for Innovation provided infrastructure for fluorescence imaging and densitometry to the Montreal Integrated Genomics Group for Research on Infectious Pathogens. The Sheldon Biotechnology Centre at McGill University is supported by a multi-user maintenance grant from Canadian Institutes of Health Research. The costs of publication of this article were defrayed in part by the payment of page charges. This article must therefore be hereby marked "*advertisement*" in accordance with 18 U.S.C. Section 1734 solely to indicate this fact.

‡ To whom correspondence should be addressed: Dept. of Microbiology and Immunology, Rm. 403, McGill University, 3775 University St., Montreal, Quebec H3A 2B4, Canada. Tel.: 514-398-3929; Fax: 514-398-7052; E-mail: james.coulton@mcgill.ca.

rel domain and apices of the cork domain (9). Disruption of siderophore binding to the receptor may result from TonB interactions, shifting the cork apices toward the periplasm. When viewed along the barrel axis, a previously identified 10-Å solvent-accessible channel (2), now referred to as the putative siderophore transport pathway, connects the extracellular environment to the periplasm. Conformational changes in loops of the cork domain could result in sufficient widening of this pathway to accommodate ferrichrome. Highly conserved residues along the inner barrel wall of the putative siderophore transport pathway may facilitate the diffusion of ferrichrome through FhuA by a series of low affinity binding interactions. Such a mechanism was shown for diffusion of maltose and maltodextrins along the greasy slide of LamB porin (10).

Conversely, complete or partial removal of the cork domain could expose the lumen of the barrel and allow diffusion of siderophores (11). Experiments comparing the structure and function of wild-type FhuA with FhuA containing N-terminal deletions (FhuAΔ21–128) indicate that the cork domain contributes to overall protein stability (12). The cork domain is stabilized within the barrel by an extensive network of hydrogen bonds and salt bridges, rendering complete removal of the cork during ferrichrome transport energetically unfavorable (1, 6, 13, 14). However, recent molecular dynamics simulations suggest that solvation of polar interactions within this network can reduce the energy expenditure necessary for cork removal (15). Deletions of the cork domains from the outer membrane receptors FhuA and FecA result in decreased affinity for siderophores, but retention of TonB-dependent functions (4, 12). It has been postulated that displacement of the siderophore from its initial binding site drives an inward motion of the extracellular loops, resulting in removal of the cork from the barrel lumen (4). In this model, the siderophore could pass through a transiently formed pathway by diffusion. It has even been suggested that the cork domain may physically import bound ligands through the barrel during its own translocation into the periplasm (6, 16).

Despite many mutational studies and crystal structures generated in recent years, the mechanism of siderophore transport through FhuA is poorly understood. In this study, site-directed disulfide cross-linking was used to assess the role of the cork domain during transport of the ferrichrome analog ferricrocin. Selected amino acids along the putative siderophore transport pathway (Leu^{109} and Gln^{112} in the cork domain and Ser^{356} and Met^{383} in the barrel domain) were mutated to cysteine residues to allow disulfide bond formation in the presence of an oxidative catalyst. Disulfide tethering of barrel and cork domains was predicted to limit siderophore uptake either by blocking the putative siderophore transport pathway or by preventing the removal of the cork domain. Instead, we observed levels of ferricrocin uptake comparable with untethered FhuA. Our data suggest that uptake does not require displacement of the cork domain and that siderophores transit the FhuA receptor through a route other than the putative siderophore transport pathway.

MATERIALS AND METHODS

Chemicals and Reagents—The antibiotics ampicillin and tetracycline were obtained from Sigma, as were *N*-ethylmaleimide, copper sulfate, and 1,10-phenanthroline. Other materials were Oregon Green maleimide (OGM)[1] from Molecular Probes, Inc., restriction enzymes AvrII and MluI and T4 DNA ligase from New England Biolabs Inc., and radiolabeled $^{55}FeCl_3$ from PerkinElmer Life Sciences.

Bacterial Strains, Plasmids, and Media—*E. coli* strain AW740 (*hisG4 thr-1 fhuA31 tsx-78* Δ*ompF zcb*::Tn*10* Δ*ompC*) harboring plasmid pHX405, which expresses FhuA plus a hexahistidine tag at residue 405, was used for thiol-specific fluorescent labeling experiments (17). *E. coli* strain SG303*fhuA* (MC4100 *aroB* T5-resistant) (18) harboring plasmid pPM18 (19) and encoding the *fhuACDB* genes was used for iron uptake assays. Both plasmids are derivatives of the pBR322 replicon. *E. coli* AW740 cultures were grown in LB broth (Fisher) supplemented with 125 μg/ml ampicillin and 10 μg/ml tetracycline. *E. coli* SG303*fhuA* cultures were grown in TY medium (8 g/liter Tryptone (Fisher), 5 g/liter Bacto yeast extract (Difco), and 5 g/liter NaCl) supplemented with 125 μg/ml ampicillin.

Construction of Cysteine FhuA Mutants—Residues within the putative siderophore transport pathway were selected for cysteine mutagenesis by exploiting the molecular modeling program SSBOND (20). Beginning with a Protein Data Bank file, the program identifies candidate residue pairs for disulfide formation by sampling all possible dihedral angles and atomic distances. Six single cysteine mutations (L109C, Q112C, D336C, S356C, M383C, and W451C) were created by PCR mutagenesis of plasmid pHX405 using the QuikChange site-directed mutagenesis kit (Stratagene). For all mutants, base changes were confirmed by nucleotide sequencing (Sheldon Biotechnology Centre, McGill University). Mutant plasmids transformed into *E. coli* AW740 were used for labeling studies. Each cysteine mutant plasmid was doubly digested with the restriction enzymes MluI and AvrII and then ligated into the backbone of the pPM18 vector that had been cut with the same enzymes. These recombinant plasmids were transformed into *E. coli* SG303 for iron uptake assays.

Labeling with Thiol-specific Reagents—Bacterial cell cultures were grown at 37 °C in LB broth containing 125 μg/ml ampicillin and 20 μg/ml tetracycline to A_{600} = 0.5. Cells were harvested and suspended to A_{600} = 2.5, and 250-μl aliquots were transferred into microcentrifuge tubes. Cells were pelleted and suspended in Buffer A (50 mM KH_2PO_4 and 100 mM K_2SO_4 (pH 7.0)) (21), followed by the addition of 5 mM OGM in 50 mM KH_2PO_4 (pH 9.0). After a 15-min incubation at room temperature, excess OGM was quenched by the addition of 2 mM 2-mercaptoethanol. Cells were washed twice with Buffer A, and outer membrane vesicles (OMV) were isolated as described previously (22). Briefly, harvested cells were suspended in 0.2 M Tris-HCl (pH 8.0), followed by the sequential addition of 0.2 M Tris-HCl (pH 8.0) and 1.0 M sucrose, 10 mM EDTA (pH 8.0), 2 mg/ml lysozyme, and distilled water. After formation of spheroplasts, membranes were extracted with 2% Triton X-100, 10 mM $MgCl_2$, 50 mM Tris-HCl (pH 8.0), and 1 mg/ml each DNase and RNase. Pelleted outer membrane fractions were washed three times with water prior to SDS-PAGE analysis. Labeling with 5 mM OGM was also conducted directly on OMV and on outer membrane proteins (OMP) that had been extracted from vesicles by 0.1% *N*,*N*-dimethyldodecylamine *N*-oxide. Labeling with 100 mM *N*-ethylmaleimide (NEM) was carried out with all three FhuA preparations (intact cells, OMV, and OMP) under the same conditions as with OGM. Preparations without or with NEM labeling were denatured in nonreducing (no 2-mercaptoethanol) sample buffer, followed by 5 mM OGM. Thiol-specific labeling of all three FhuA preparations was also assessed after the addition of 1.0 μM ferricrocin and 0.5% glucose. An ~20:1 molar ratio of thiol-specific probe to FhuA was used for all labeling experiments.

^{55}Fe-Ferricrocin Transport Assay and Disulfide Cross-linking—Bacterial cells were grown overnight in TY medium and then transferred to 10 ml of fresh TY medium until A_{578} = 0.4 was reached. Cells were washed with iron uptake medium (10 mM Tris-HCl (pH 7.2), 0.5% glucose, and 1.0 mM $MgSO_4$) and then suspended in 10 ml of iron uptake medium with 100 μM nitrilotriacetate. $^{55}FeCl_3$ was complexed with desferrated ferricrocin in equimolar ratios and incubated for several minutes at room temperature. Bacteria were incubated at 37 °C for 5 min in a shaking water bath prior to ^{55}Fe-ferricrocin uptake or to oxidative cross-linking. Following the addition of 1.0 μM ^{55}Fe-ferricrocin, 1.0-ml samples were removed at 5-min intervals, collected on 0.45-μm nitrocellulose filters (Millipore Corp.), and washed twice with 0.1 mM LiCl. Filters were dried and counted in a Packard Tri-Carb 2100TR liquid scintillation analyzer.

For cells containing double cysteine FhuA mutants, disulfide bond formation was enhanced by the addition of an oxidative catalyst. Specifically, cells were incubated at 37 °C for 10 min with 100 μM copper(II) phenanthroline (CuP) or with 50 μM copper sulfate ($CuSO_4$) either before or after initiation of ^{55}Fe-ferricrocin uptake.

SDS-PAGE, Western Immunoblotting, and Fluorescence Imaging—Cellular proteins were resolved by SDS-PAGE on gels containing 10% acrylamide. For OGM labeling experiments, gels were scanned for fluorescence using a Bio-Rad FX scanner. Following cross-linking and uptake assays, proteins were transferred from acrylamide gels to Immobilon-P transfer membranes (Millipore Corp.) overnight at 38 mA in

[1] The abbreviations used are: OGM, Oregon Green maleimide; OMV, outer membrane vesicles; OMP, outer membrane proteins; NEM, *N*-ethylmaleimide; CuP, copper(II) phenanthroline.

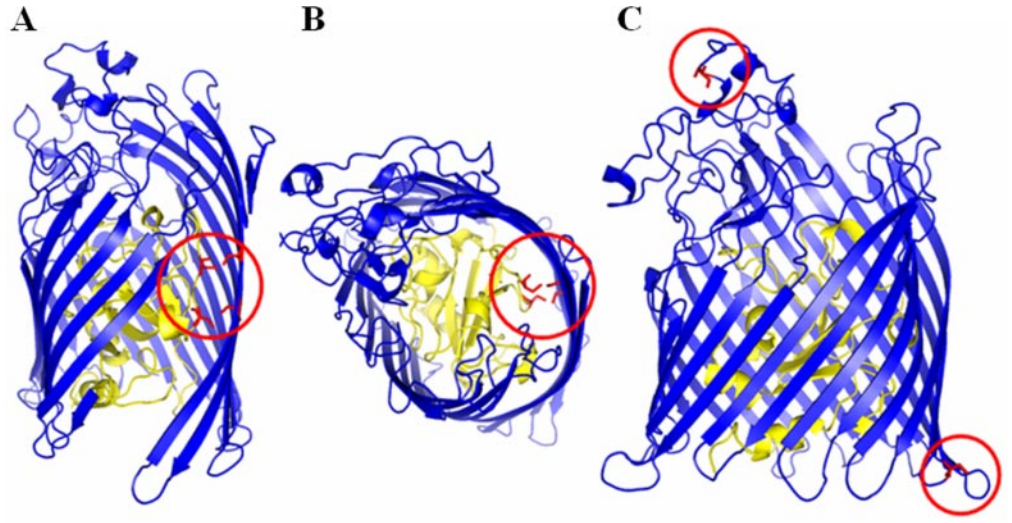

FIG. 1. **Outer membrane receptor FhuA.** *A*, side view of FhuA in ribbon representation. The barrel domain (in *blue*) is shown with residues 438–467 and 480–490 removed to allow unobstructed views of the putative siderophore transport pathway and cork domain (in *yellow*). Four single cysteine mutants are represented as *red stick models*: L109C (*lower*) and Q112C (*upper*) in the cork domain and S356C (*lower*) and M383C (*upper*) in the barrel domain. *B*, FhuA as viewed from the external environment along the barrel axis. The orientation of the cysteine mutant side chains, shown as *red stick models*, can be visualized in the putative siderophore transport pathway. *C*, two control cysteine mutations in the surface-exposed and periplasmic environments: D336C (*upper*) located in loop L4 and W451C (*lower*) located in periplasmic turn T5.

a 4 °C cold chamber by electrophoresis in transfer buffer (48 mM Tris-HCl (pH 8.3), 39 mM glycine, 0.04% SDS, and 20% methanol). Membranes were blocked in 30 ml of Tris-buffered saline (20 mM Tris-HCl (pH 7.3) and 150 mM NaCl) containing 2% bovine serum albumin for 1 h at room temperature. The blocking buffer was used to dilute both the primary monoclonal antibody FhuA4.1 (18) and the secondary antibody coupled to alkaline phosphatase (Cedarlane Laboratories Ltd.). Membranes incubated with a 1:1000 dilution of antibody FhuA4.1 for 1 h at room temperature were washed three times for 5 min with Tris-buffered saline containing 0.1% Tween 20 and then treated in a similar manner with a 1:8000 dilution of alkaline phosphatase. After washing, blots were developed using nitro blue tetrazolium/5-bromo-4-chloro-3-indolyl phosphate developing reagents (Roche Diagnostics) in 100 mM $NaHCO_3$ and 1.0 mM $MgCl_2$. The reaction was stopped by the addition of water. Immunoblots were scanned with a Bio-Rad FX scanner, followed by densitometry using Bio-Rad Quantity One software to quantitate the percentage of disulfide bond formation in the double cysteine FhuA mutants.

RESULTS

Engineering Cysteine Mutants within the Putative Siderophore Transport Pathway—To evaluate the role of specific amino acids within the putative siderophore transport pathway of FhuA, site-directed mutagenesis was undertaken. Our objectives were to engineer disulfide bonds that tethered the cork and barrel domains and to create a barrier within the putative siderophore transport pathway. Using the FhuA crystal structure (Protein Data Bank code 2FCP) as input, the molecular modeling program SSBOND (20) identified candidate amino acids for mutagenesis to cysteine residues. Based on the proximity and side chain orientation of residues in the crystal structure, SSBOND predicted their propensity to form disulfide bonds. Two single cysteine mutants (L109C and Q112C) were created in the cork domain, and two others were created in β-strands 8 (S356C) and 9 (M383C) of the barrel domain (Fig. 1*A*). Given these selections, SSBOND predicted disulfide formation for the double cysteine mutants L109C/S356C and Q112C/M383C (Fig. 1*B*).

Thiol-specific Labeling of Putative Siderophore Transport Pathway Cysteine Mutants—The accessibility of four cysteine mutants (L109C, Q112C, S356C, and M383C) within the putative siderophore transport pathway was evaluated by reactivity of their sulfhydryl groups with the thiol-specific probe OGM. The additional FhuA mutants D336C (located in surface-exposed loop L4) and W451C (located in periplasmic turn T5) were created as controls to probe for surface accessibility and periplasmic accessibility, respectively (Fig. 1*C*). *E. coli* AW740 was transformed with plasmids encoding wild-type FhuA, single cysteine FhuA mutants (L109C, Q112C, D336C, M383C, and W451C), or double cysteine FhuA mutants (L109C/S356C and Q112C/M383C). *E. coli* transformants were used for intact cell labeling experiments with OGM; alternatively, OMV and detergent-solubilized OMP were labeled with OGM. SDS-polyacrylamide gels were scanned to detect the fluorescent modification of sulfhydryl groups with OGM. In both intact cells and OMV, only Cys^{336} in surface-exposed loop L4 was modified with OGM (Fig. 2, *A* and *B*). Cysteine mutants in the putative siderophore transport pathway were not labeled, indicating that OGM did not have access to the barrel lumen of FhuA. Consequently, assessment of disulfide bond formation in the double cysteine mutants L109C/S356C and Q112C/M383C could not be conducted by fluorescent labeling. Whereas periplasmic turn T5 residue Cys^{451} was not accessible to OGM in intact cells or OMV, FhuA residue Cys^{451} became accessible to OGM modification once OMP were extracted in 0.1% *N*,*N*-dimethyldodecylamine *N*-oxide (Fig. 2*C*).

Initial labeling with NEM was predicted to prevent subsequent reaction with OGM. In all three FhuA preparations, labeling with NEM blocked OGM modification of Cys^{336}. NEM labeling of detergent-solubilized W451C also blocked subsequent reaction with OGM (Fig. 3). Thiol-specific labeling assays with OGM or NEM/OGM were conducted during ferricrocin transport; identical labeling outcomes were observed for intact cells, OMV, and detergent-solubilized OMP compared with FhuA not transporting ligand (data not shown).

Analysis of Double Cysteine FhuA Mutants by Nonreducing SDS-PAGE—To determine whether intact cells expressing double cysteine FhuA mutants are able to form predicted disulfide bonds within the putative siderophore transport pathway, FhuA was denatured under nonreducing conditions, followed by labeling with OGM. Upon denaturation of FhuA, all mutated cysteine residues (Cys^{109}, Cys^{112}, Cys^{336}, Cys^{356}, Cys^{383}, and Cys^{451}) were accessible to OGM, whereas wild-type FhuA remained unmodified (Fig. 4*A*, *upper panel*). Analyses of cells containing double cysteine FhuA mutants by SDS-PAGE under nonreducing conditions displayed a mixture of two distinct species: FhuA in which the disulfide bond had formed and

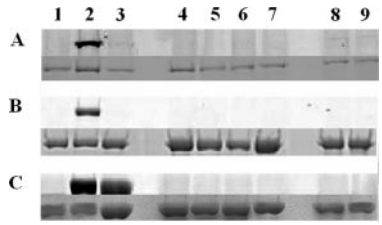

FIG. 2. **OGM labeling of cysteine FhuA mutants.** The *upper panels* represent fluorescence scans of labeled proteins after nonreducing SDS-PAGE; the corresponding Coomassie Blue staining is shown in the *lower panels*. *A*, labeling of intact cells before extracting OMV; *B*, labeling of OMV; *C*, labeling of OMP solubilized by 0.1% *N*,*N*-dimethyldodecylamine *N*-oxide from OMV. *Lanes 1*, wild-type FhuA; *lanes 2*, D336C; *lanes 3*, W451C; *lanes 4*, L109C; *lanes 5*, Q112C; *lanes 6*, S356C; *lanes 7*, M383C; *lanes 8*, L109C/S356C; *lanes 9*, Q112C/M383C.

FIG. 3. **NEM labeling of cysteine FhuA mutants, followed by reaction with OGM.** The *upper panel* represents a fluorescence scan of labeled proteins after nonreducing SDS-PAGE; the corresponding Coomassie Blue staining is shown in the *lower panel*. Shown is the labeling of OMP solubilized by 0.1% *N*,*N*-dimethyldodecylamine *N*-oxide from OMV. *Lane 1*, wild-type FhuA; *lane 2*, D336C; *lane 3*, W451C; *lane 4*, L109C; *lane 5*, Q112C; *lane 6*, S356C; *lane 7*, M383C; *lane 8*, L109C/S356C; *lane 9*, Q112C/M383C.

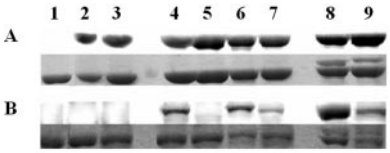

FIG. 4. **Nonreducing denaturation of cysteine FhuA mutants, followed by thiol-specific labeling.** The *upper panels* represent fluorescence scans of labeled proteins after nonreducing SDS-PAGE; the corresponding Coomassie Blue staining is shown in the *lower panels*. *A*, OGM labeling; *B*, NEM labeling, followed by reaction with OGM. *Lanes 1*, wild-type FhuA; *lanes 2*, D336C; *lanes 3*, W451C; *lanes 4*, L109C; *lanes 5*, Q112C; *lanes 6*, S356C; *lanes 7*, M383C; *lanes 8*, L109C/S356C; *lanes 9*, Q112C/M383C.

FhuA containing free sulfhydryl groups (Fig. 4, *A* and *B*, *lower panels*). The faster migrating and more abundant species indicated by the lower band was modified by fluorescent labeling, indicating free sulfhydryl groups. The upper band (Fig. 4*A*, *lanes 8* and *9*) corresponding to the slower migrating and less abundant species could not be fluorescently modified, signifying the presence of disulfide bonds. When wild-type FhuA was denatured in the presence or absence of reducing agent, the resulting proteins displayed similar electrophoretic mobilities. Double cysteine FhuA mutants electrophoresed under reducing conditions were fully denatured, resulting in one band with mobility identical to that of wild-type FhuA. FhuA samples initially labeled with NEM and then analyzed by nonreducing SDS-PAGE revealed that NEM modified the surface-exposed mutant D336C, periplasmic mutant W451C, and putative siderophore transport pathway mutant Q112C (Fig. 4*B*, *upper panel*) because subsequent OGM labeling was not observed.

Oxidative Cross-linking of Double Cysteine FhuA Mutants—To ensure maximal disulfide bond formation during ferricrocin transport assays, we employed an oxidative catalyst that promotes cross-linking. Treatment of cells with an oxidative catalyst has been shown to enhance disulfide bond formation between appropriately positioned cysteine thiols (21). Cross-linking the sulfhydryl groups of the mutated double cysteine residues can be accomplished with zero-length cross-linkers such as CuP and $CuSO_4$. The oxidative catalyst CuP

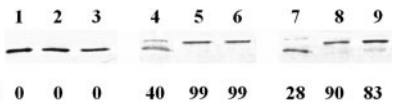

FIG. 5. **Oxidative cross-linking of FhuA.** Intact cells expressing wild-type FhuA (*lanes 1–3*), L109C/S356C (*lanes 4–6*), and Q112C/M383C (*lanes 7–9*) were treated with an oxidative catalyst for 10 min at 37 °C. Following Western blot analysis, disulfide formation was assessed by scanning densitometry. The percentage of FhuA containing a disulfide bond (*S–S*) is indicated for each treatment. *Lanes 1*, *4*, and *7*, no oxidation; *lanes 2*, *5*, and *8*, CuP treatment; *lanes 3*, *6*, and *9*, $CuSO_4$ treatment.

has been extensively reported to enhance disulfide bond formation between transmembrane domains of membrane proteins (23–27). To achieve maximal disulfide formation in our double cysteine FhuA mutants, intact cells suspended in iron uptake medium were treated with an oxidative catalyst (CuP or $CuSO_4$). To calculate the relative proportions of FhuA containing disulfide bonds under these conditions, the cross-linked samples were resolved by nonreducing SDS-PAGE and Western blot analysis, followed by densitometry. Cross-linking between the cork and barrel domains in double cysteine FhuA mutants was apparent from the reduced electrophoretic mobilities of cross-linked species compared with protein containing free sulfhydryl groups. Cross-linked protein was not detected in wild-type FhuA (Fig. 5) or in any single cysteine mutant (data not shown). Oxidation with CuP yielded 99 and 90% disulfide-formed species for L109C/S356C and Q112C/M383C, respectively (Fig. 5). Replacing CuP with $CuSO_4$ as the cross-linking agent resulted in nearly equivalent efficiencies of disulfide formation in cells expressing L109C/S356C (99%) and Q112C/M383C (83%) (Fig. 5).

^{55}Fe-Ferricrocin Uptake in Cells Expressing Cysteine FhuA Mutants—Strains expressing single and double cysteine FhuA mutants were assayed for their ability to transport the iron-ferricrocin complex. FhuA and the FhuCDB accessory proteins required for transport were expressed in the *aroB* mutant *E. coli* SG303 strain. The *aroB* mutant strain prevented endogenous synthesis of enterochelin, which might chelate radiolabeled ^{55}Fe in transport assays. Iron uptake by wild-type FhuA was measured as 56.2 pmol of ^{55}Fe-ferricrocin/10^8 cells over a period of 25 min. Both single cysteine mutants L109C and M383C exhibited 95% ^{55}Fe-ferricrocin uptake of wild-type FhuA (Fig. 6). Q112C and S356C transported 68 and 84% ^{55}Fe-ferricrocin, respectively, compared with wild-type levels (Fig. 6). Both double cysteine FhuA mutants also showed decreased levels of transport; L109C/S356C transported 68% of the wild-type levels, whereas Q112C/M383C transported 75% (Fig. 6). These results demonstrate reduced transport of ^{55}Fe-ferricrocin into cells expressing double cysteine FhuA mutants. However, under these non-oxidized conditions, cells containing L109C/S356C and Q112C/M383C formed only 40 and 28% disulfide-formed species, respectively (Fig. 5).

^{55}Fe-Ferricrocin Uptake in Oxidized Double Cysteine FhuA Mutants—To test whether cross-linking of the cork to the barrel would affect siderophore uptake by FhuA, cells were first treated with an oxidative catalyst to maximize disulfide formation before the addition of the ^{55}Fe-ferricrocin complex. Although CuP was capable of cross-linking double cysteine residues to nearly 100%, it had an unfavorable effect on siderophore uptake, reducing wild-type transport by 3-fold (data not shown). It has been shown that Fe^{3+} can effectively compete with Fe^{2+} for binding to 1,10-phenanthroline in solution (28). In this case, the reduction in transport may have been due to competition for $^{55}Fe^{3+}$ binding between ferricrocin and 1,10-phenanthroline, resulting in the uptake of apoferricrocin.

Given the effects of CuP, wild-type, single cysteine, double

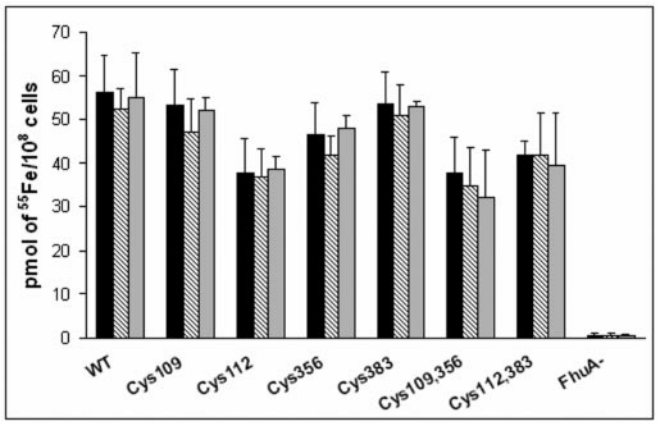

FIG. 6. **Transport of ^{55}Fe-ferricrocin by cysteine FhuA mutants of *E. coli*.** Cells were grown in TY medium and tested for uptake of ^{55}Fe-ferricrocin over 25 min. FhuA mutant strains were tested in the absence of oxidation (*black bars*), after oxidation (*hatched bars*), and after oxidation during ^{55}Fe-ferricrocin transport (*gray bars*). *Error bars* indicate S.D. from mean transport levels of three independent experiments. *WT*, wild-type FhuA.

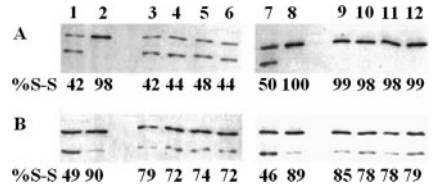

FIG. 7. **Disulfide bond formation in double cysteine FhuA mutants during ferricrocin transport.** Intact cells expressing L109C/S356C (*A*) and Q112C/M383C (*B*) were sampled at 5-min intervals during ferricrocin transport (*lanes 3–6*) and sampled at 5-min intervals after treatment with $CuSO_4$ at 37 °C after a 5-min initiation of ferricrocin transport (*lanes 9–12*). The percentage of FhuA containing a disulfide bond (*S–S*) was assessed by Western blot analysis and densitometry. *Lanes 1* and *7*, no oxidation; *lanes 2* and *8*, $CuSO_4$ treatment; *lanes 3* and *9*, 10 min of transport; *lanes 4* and *10*, 15 min of transport; *lanes 5* and *11*, 20 min of transport; *lanes 6* and *12*, 25 min of transport.

cysteine, and FhuA-deleted strains were instead oxidized with $CuSO_4$ to promote disulfide bond formation. Aliquots of cells were removed over 25 min, and the amount of ^{55}Fe-ferricrocin taken into the cells was determined by liquid scintillation analysis. ^{55}Fe-ferricrocin uptake by wild-type FhuA in the presence of the oxidative catalyst retained 93% transport activity (Fig. 6). All four single cysteine FhuA mutants located within the putative siderophore transport pathway also retained their ability to transport ferricrocin after oxidation: L109C, 88%; Q112C, 96%; S356C, 90%; and M383C, 95% (Fig. 6). Despite nearly complete disulfide formation, L109C/S356C and Q112C/M383C transported 34.8 and 41.5 pmol of ^{55}Fe-ferricrocin/10^8 cells, respectively. Therefore, these double cysteine mutants were proficient for transport of ferricrocin at levels of 93 and 99%, respectively, compared with non-oxidized double cysteine FhuA mutants (Fig. 6). Engineered disulfide bonds obstructing the putative siderophore transport pathway did not prevent ferricrocin transport through FhuA.

Disulfide Bond Formation in Double Cysteine FhuA Mutants during ^{55}Fe-Ferricrocin Transport—We investigated whether siderophore transport might interfere with cross-linking of L109C/S356C and Q112C/M383C within the putative siderophore transport pathway. Siderophore transport of non-oxidized cells expressing L109C/S356C did not increase the levels of disulfide bond formation (Fig. 7*A*, *lanes 3–6*). In contrast, non-oxidized cells expressing Q112C/M383C exhibited increased disulfide bond formation during ferricrocin transport (Fig. 7*B*, *lanes 3–6*). After 25 min of ferricrocin transport, the level of cross-linking displayed in Q112C/M383C was similar in the presence (79%) and absence (72%) of oxidant (Fig. 7*B*, *lanes 6* and *12*).

Double cysteine FhuA mutants preincubated with ^{55}Fe-ferricrocin before the addition of an oxidative catalyst did not exhibit reduced disulfide formation upon oxidation (Fig. 7*B*). Cross-linking occurred at the previously observed rates, reaching their maxima after a 5-min incubation with $CuSO_4$ (equivalent to 10 min of ^{55}Fe-ferricrocin transport). During ferricrocin transport, disulfide formation catalyzed by $CuSO_4$ in L109C/S356C increased from 50 to 99%; Q112C/M383C increased disulfide-formed species from 46 to 85% (Fig. 7*B*). Despite attachment of the cork to the barrel and obstruction of the putative siderophore transport pathway, there was no significant difference in ferricrocin transport, with levels of 32.2 (L109C/S356C) and 39.4 (Q112C/M383C) pmol of ^{55}Fe-ferricrocin/10^8 cells over 25 min (Fig. 6). These results establish that, during ferricrocin transport, regions of the cork domain around residues 109–112 remain in close proximity to the inner barrel wall along the putative siderophore transport pathway.

DISCUSSION

The molecular mechanism for siderophore transport through TonB-dependent OM receptors is currently unknown. Proposed models have suggested partial or complete removal of the cork domain from the barrel during siderophore passage (1, 4–6). FhuA crystal structures in the absence and presence of bound siderophore do not completely describe conformational changes during energy transduction and siderophore transport. Therefore, *in vivo* and *in vitro* strategies are required to provide insights concerning possible displacement of the cork domain during transport. After identifying candidate disulfide-forming residues in the FhuA crystal structure (2), FhuA mutations in the cork domain (L109C and Q112C) and in the barrel domain (S356C and M383C) were constructed. The two prevailing models of siderophore transport, expansion of the putative siderophore transport pathway and displacement of the cork domain, could be tested by forming disulfide cross-links between the cork and barrel domains within this region.

To assess formation of disulfide bonds predicted by molecular modeling and accessibility of the introduced cysteines, thiol-specific labeling with fluorescent reagents was employed; conformational changes during ferricrocin transport were also monitored. Only Cys^{336} on surface-exposed loop L4 of FhuA was labeled with OGM, whereas the four cysteine residues within the putative siderophore transport pathway (Cys^{109}, Cys^{112}, Cys^{356}, and Cys^{383}) and a cysteine located in a periplasm-oriented turn (Cys^{451}) remained unmodified (Fig. 2). Labeling assays with the membrane-impermeable thiol-specific probe 5-iodoacetamidofluorescein (515 Da) provided accessibility results identical to those obtained with membrane-permeable OGM (data not shown). OGM (463 Da) gains access to the periplasm by permeating the outer membrane through porins. Previous studies demonstrated OGM labeling of periplasm-exposed regions of the cytoplasmic membrane-bound proteins TonB (21) and OxlT (29, 30). Unexpectedly, our periplasmic control, Cys^{451}, was not accessible to OGM in intact cells or on OMV without prior denaturation of FhuA. After detergent extraction from OMV, Cys^{451} became accessible to thiol modification with OGM. Conversely, the smaller compound NEM (125 Da) was capable of reaction with Cys^{451} in all three FhuA preparations. Therefore, the presence of the lipid bilayer apparently inhibits modification of Cys^{451} with the bulkier thiol-specific reagent OGM. Amino acids exposed to the lipid bilayer have higher pK_a values that correlate with low reactivity by maleimides (29, 30). These observations were substantiated by elevated concentrations of NEM required to

label Cys^{451} in the short periplasmic turn. Accessibility of Cys^{336} to maleimide modification is in agreement with a study by Bös and Braun (31), although they reported that the fluorescent labeling of Cys^{336} with the thiol-specific maleimide is quenched upon ferrichrome binding, reflecting structural changes in surface-exposed loop L4. In our experiments, there were no changes in the accessibility of FhuA residue Cys^{336} or any other mutated cysteine residue of FhuA to OGM during ferricrocin transport. This implies that structural changes occurring during transport do not alter the accessibility of these mutated cysteine residues. Removal of the cork domain during transport was predicted to render cysteine mutants in the vacated barrel lumen and cork cysteine mutants in the periplasm accessible to OGM modification. However, because cells containing the four single cysteine FhuA mutants within the putative siderophore pathway were not labeled by OGM during ferricrocin transport, these results favor a mechanism whereby the cork remains within the barrel.

To determine the extent of disulfide bond formation, double cysteine FhuA mutants were denatured under nonreducing conditions; disulfide bonds formed prior to OGM labeling would not be accessible to subsequent modification. Before publication of the x-ray crystallographic structure of FhuA, the two native disulfide bonds in FhuA were identified using a similar thiol-specific labeling strategy (31). After nonreducing denaturation, wild-type FhuA was not labeled with OGM; all single cysteine FhuA mutants were accessible to labeling (Fig. 4, *A* and *B*, *lower panels*). The appearance of two distinct FhuA species in double cysteine mutants under nonreducing conditions indicated partial disulfide bond formation. The FhuA species containing engineered disulfides were unlabeled by OGM, indicating no free sulfhydryl groups; they also had lower electrophoretic mobilities on SDS-PAGE (Fig. 4). Incomplete denaturation of FhuA may be due to the large distance between thiol groups (247 residues in L109C/S356C and 271 residues in Q112C/M383C) forming the disulfide bonds, forcing the protein to retain a partial fold. Conversely, the two native disulfide bonds in FhuA, located in surface-exposed loops L4 and L11, do not interfere with unfolding during denaturation due to the small distances between thiol groups (11 residues in loop L4 and 6 residues in loop L11) (31). Discriminating between FhuA harboring disulfide bonds and FhuA containing free sulfhydryl groups was useful in assessing the outcomes of our oxidative cross-linking. Preparations containing maximally disulfide-tethered mutants were required to probe repositioning of the cork domain or enlarging of the putative siderophore transport pathway during siderophore uptake.

Based on our experiments involving oxidative cross-linking, we conclude that the cork domain is not removed from the barrel during ferricrocin transport. Double cysteine FhuA mutants readily formed disulfide bonds using the oxidative catalysts CuP and $CuSO_4$ (Fig. 5). It has been estimated that the maximal distance between the β-carbons for cross-linking cysteine residues via oxidation is 7 Å and is optimal between 5 and 6 Å (23). L109C/S356C and Q112C/M383C have inter-β-carbon distances of 4.22 and 4.80 Å, respectively. Disulfide tethering of the cork and barrel domains was used to probe the effect of restricting the conformational mobility of the cork domain relative to the barrel. Decreased transport of ^{55}Fe-ferricrocin seen in cells expressing double cysteine FhuA mutants was not anticipated without oxidative cross-linking; under these conditions, L109C/S356C and Q112C/M383C formed only 40 and 28% disulfide-formed species, respectively (Fig. 6). The single cysteine mutants Q112C and S356C displayed decreased transport, suggesting that these residues may interact with the barrel domain during ferricrocin transport. Therefore, the reduced uptake levels observed in both double cysteine FhuA mutants may be attributed to the decreased ^{55}Fe-ferricrocin transport by Cys^{112} and Cys^{356}, each contained in one of the double cysteine mutants (Fig. 6). Because treatment of cells with CuP was detrimental to ferricrocin transport, uptake assays of ^{55}Fe-ferricrocin were conducted on cells treated with the oxidative catalyst $CuSO_4$. Compared with siderophore uptake by cells not treated with $CuSO_4$, FhuA containing disulfide-cross-linked double cysteine mutants within the putative siderophore transport pathway remained transport-proficient (Fig. 6). Therefore, tethering of the cork domain to the barrel does not hinder conformational changes in the receptor that may accompany ferricrocin transport into the periplasm.

The ability of engineered cysteines to form disulfide bonds with variable efficiencies during transport provided additional insights into displacement(s) of the cork domain. Ferricrocin uptake through Q112C/M383C (but not L109C/S356C) dramatically increased disulfide formation in the absence of $CuSO_4$ (Fig. 7). This suggests enhanced proximity of the two putative pathway sulfhydryl groups Cys^{112} and Cys^{383} during transport. Therefore, it is unlikely that the cork moves significantly away from the barrel wall in this region to allow siderophore passage. When cells transporting ferricrocin were treated with $CuSO_4$, the extent of Q112C/M383C disulfide formation remained unchanged relative to untreated cells; however, L109C/S356C disulfide formation became more efficient (Fig. 7). Furthermore, ferricrocin transport was not affected by disulfide formation during its passage through FhuA (Fig. 6). Disulfide tethering could not occur if the cork domain were displaced into the periplasm.

Because disulfide bonds within the putative siderophore transport pathway did not inhibit ferricrocin transport through FhuA, it is likely that, upon interaction with TonB, conformational changes may open an alternative pathway. Disulfide tethering of the switch helix of the cork to periplasmic turn T7 of the barrel domain between engineered cysteines at positions 27 and 533 eliminates the transport of ferrichrome, albomycin, and microcin J25 through FhuA (8). Covalent fixation of the cork to the barrel still enables interaction with TonB, but does not allow movements in the cork to open a transport channel. Therefore, this double cysteine FhuA mutant may indicate an alternative siderophore transport pathway.

Oxidative cross-linking proved to be an effective tool to probe conformational changes during ferricrocin transport. Disulfide tethering of the cork to the barrel domain within the putative siderophore transport pathway was not sufficient to limit ferricrocin uptake. Ferricrocin uptake enhanced Q112C/M383C disulfide formation; and upon oxidative cross-linking, both double cysteine FhuA mutants completed disulfide formation through the putative siderophore transport pathway. Taken together, we conclude that the cork domain remains within close proximity to the inner barrel wall during siderophore transport. Furthermore, the siderophore likely transits the interior of the receptor through a series of low affinity interactions between both the cork domain and residues located along the inner wall of the barrel domain. Disulfide tethering of the cork and barrel domains in other regions of FhuA will lead to precise identification of the siderophore transport pathway. Elucidation of this pathway and the mechanism for siderophore transport through FhuA will provide insights into transport of ligands by other TonB-dependent outer membrane receptors.

Acknowledgments—We thank B. Cousineau, M. A. Hancock, and H. Le Moual for critically reviewing the manuscript and J. A. Kashul for editorial support.

REFERENCES

1. Klebba, P. E. (2003) *Front. Biosci.* **8,** s1422–s1436
2. Ferguson, A. D., Hofmann, E., Coulton, J. W., Diederichs, K., and Welte, W. (1998) *Science* **282,** 2215–2220
3. Locher, K. P., Rees, B., Koebnik, R., Mitschler, A., Moulinier, L., Rosenbusch, J. P., and Moras, D. (1998) *Cell* **95,** 771–778
4. Scott, D. C., Cao, Z., Qi, Z., Bauler, M., Igo, J. D., Newton, S. M. C., and Klebba, P. E. (2001) *J. Biol. Chem.* **276,** 13025–13033
5. Postle, K., and Kadner, R. J. (2003) *Mol. Microbiol.* **49,** 869–882
6. Ferguson, A. D., and Deisenhofer, J. (2004) *Cell* **116,** 15–24
7. Cadieux, N., and Kadner, R. J. (1999) *Proc. Natl. Acad. Sci. U. S. A.* **96,** 10673–10678
8. Endriss, F., Braun, M., Killmann, H., and Braun, V. (2003) *J. Bacteriol.* **185,** 4683–4692
9. Braun, V., and Braun, M. (2002) *FEBS Lett.* **529,** 78–85
10. Van Gelder, P., Dumas, F., Bartoldus, I., Saint, N., Prilipov, A., Winterhalter, M., Wang, Y., Philippsen, A., Rosenbusch, J. P., and Schirmer, T. (2002) *J. Bacteriol.* **184,** 2994–2999
11. Braun, M., Killmann, H., and Braun, V. (1999) *Mol. Microbiol.* **33,** 1037–1049
12. Bonhivers, M., Desmadril, M., Moeck, G. S., Boulanger, P., Colomer-Pallas, A., and Letellier, L. (2001) *Biochemistry* **40,** 2606–2613
13. Chimento, D. P., Mohanty, A. K., Kadner, R. J., and Wiener, M. C. (2003) *Nat. Struct. Biol.* **10,** 394–401
14. Buchanan, S. K., Smith, B. S., Venkatramani, L., Xia, D., Esser, L., Palnitkar, M., Chakraborty, R., van der Helm, D., and Deisenhofer, J. (1999) *Nat. Struct. Biol.* **6,** 56–63
15. Faraldo-Gomez, J. D., Smith, G. R., and Sansom, M. S. (2003) *Biophys. J.* **85,** 1406–1420
16. Usher, K. C., Özkan, E., Gardner, K. H., and Deisenhofer, J. (2001) *Proc. Natl. Acad. Sci. U. S. A.* **98,** 10676–10681
17. Moeck, G. S., Tawa, P., Xiang, H., Ismail, A. A., Turnbull, J. L., and Coulton, J. W. (1996) *Mol. Microbiol.* **22,** 459–471
18. Moeck, G. S., Ratcliffe, M. J. H., and Coulton, J. W. (1995) *J. Bacteriol.* **177,** 6118–6125M. J. H.
19. Coulton, J. W., Mason, P., and DuBow, M. S. (1983) *J. Bacteriol.* **156,** 1315–1321
20. Hazes, B., and Dijkstra, B. W. (1988) *Protein Eng.* **2,** 119–125
21. Larsen, R. A., Letain, T. E., and Postle, K. (2003) *Mol. Microbiol.* **49,** 211–218
22. Hantke, K. (1981) *Mol. Gen. Genet.* **182,** 288–292
23. Loo, T. W., Bartlett, M. C., and Clarke, D. M. (2004) *J. Biol. Chem.* **279,** 18232–18238
24. Loo, T. W., Bartlett, M. C., and Clarke, D. M. (2004) *J. Biol. Chem.* **279,** 7692–7697
25. Chervitz, S. A., and Falke, J. J. (1995) *J. Biol. Chem.* **270,** 24043–24053
26. Aziz, Q. H., Partridge, C. J., Munsey, T. S., and Sivaprasadarao, A. (2002) *J. Biol. Chem.* **277,** 42719–42725
27. Hughson, A. G., and Hazelbauer, G. L. (1996) *Proc. Natl. Acad. Sci. U. S. A.* **93,** 11546–11551
28. Fadrus, H., and Maly, J. (1975) *Analyst* **100,** 549–554
29. Fu, D., Sarker, R. I., Abe, K., Bolton, E., and Maloney, P. C. (2001) *J. Biol. Chem.* **276,** 8753–8760
30. Ye, L., Jia, Z., Jung, T., and Maloney, P. C. (2001) *J. Bacteriol.* **183,** 2490–2496
31. Bös, C., and Braun, V. (1997) *FEMS Microbiol. Lett.* **153,** 311–319